FEELING THE PULSE OF THE STRATOSPHERE

An Emerging Opportunity for Predicting Continental-Scale Cold-Air Outbreaks 1 Month in Advance

BY MING CAI, YUEYUE YU, YI DENG, HUUG M. VAN DEN DOOL, RONGCAI REN, SURU SAHA, XINGREN WU, AND JIN HUANG

The linkage of the occurrence probability of continental-scale cold-air outbreaks to the amount of air mass transported into the polar stratosphere suggests that it is feasible to predict them 1 month in advance.

Past studies have linked the weakening of the stratospheric polar vortex or the negative phase of the northern annular mode (NAM) to episodes of extreme cold events that occur later in the midlatitudes (Thompson and Wallace 2001; Baldwin and Dunkerton 2001; Thompson et al. 2002; Cai 2003; Kolstad et al. 2010; Mitchell et al. 2013; Kidston et al. 2015). The presence of the NAM variability in the lower stratosphere also provides enhanced predictability of the Arctic Oscillation (AO) or the tropospheric NAM variability (Baldwin et al. 2003; Kuroda 2008; Douville 2009; Gerber et al. 2009; Hardiman et al. 2011; Smith et al. 2012; Sigmond et al. 2013; Tripathi et al. 2014). This enhanced predictability has been attributed to the dynamical coupling between the stratosphere and troposphere via 1) systematic downward propagation of geopotential height and zonal wind anomalies in the extratropics (Kodera and Kuroda 1990; Baldwin and Dunkerton 1999; Baldwin and Dunkerton 2001; Cai and Ren 2007; Ren and Cai 2007), 2) the delayed feedbacks of the stratosphere to the upward propagation of tropospheric Rossby waves (Hartley et al. 1998; Limpavusan and Hartmann 2000; Ambaum and Hoskins 2002; Polvani and Waugh 2004; Kuroda 2008), 3) the downward control principle (Haynes et al. 1991) and with transient eddy feedbacks (Song and Robinson 2004), 4) the reflection of planetary waves (Perlwitz and Harnik 2003), and 5) the invertibility principle of potential vorticity (Hartley et al. 1998). Readers may consult the monumental review papers by Holton et al. (1995), Shepherd (2002), and Haynes (2005), and the references therein, about the two-way coupling mechanisms between the stratosphere and troposphere in the extratropics. The stratospheric connection to the AO and the associated extreme weather events have been recognized as a new opportunity for intraseasonal climate predictions during winter seasons since the stratospheric signal provides long-lead precursor information (0–60 days) to anomalous surface regimes (Baldwin and Dunkerton 2001; Thompson and Wallace 2001; Baldwin et al. 2003; Polvani and Waugh 2004).

The conventional wisdom is that the stratosphere is more predictable than the troposphere because of its longer persistent time scale from the dominance of the quasi-stationary planetary-scale Rossby waves over the fast-moving synoptic-scale waves. With more satellite data in the stratosphere to assimilate and increased vertical resolution, we now have the capability to use numerical weather prediction (NWP)

models as an initial-value problem for stratospheric forecasts in the extratropics with a useful degree of skill in the subseasonal range [e.g., Tripathi et al. (2014) for extreme polar vortex events; Christiansen (2005), Charlton and Polvani (2007), and Yoden et al. (2014) for major stratospheric sudden warming events; Marshall et al. (2009) for a rare volcanic eruption event; Stan and Straus (2009), Li and Ding (2011), and Zhang et al. (2013) for zonal mean temperature, geopotential height, and wind anomalies]. The findings of these studies indicate that the useful skill for subseasonal forecasts in the extratropical stratosphere is due to the models' ability to retain the amplitude of planetary waves throughout the subseasonal range, despite the fact that the models may not be able to predict the exact locations of planetary waves and their spatial scales beyond the 2-week range. It has been suggested that the skill improvement in the subseasonal range also depends on the initial day of the forecast relative to the onset date of the stratospheric sudden warming events (Kuroda 2010), and skillful subseasonal forecasts for extratropical stratospheric anomalies are not found for all cases (Tripathi et al. 2014). Sigmond et al. (2013) further showed that model forecasts for monthly mean tropospheric anomalies have significantly greater skill in the months after stratospheric sudden warming events. The skill dependency on the initial conditions in the stratosphere suggests that models can capture the long-lead information between stratospheric and tropospheric anomalies.

AFFILIATIONS: Cai—Department of Earth, Ocean and Atmospheric Sciences, Florida State University, Tallahassee, Florida; Yu—Department of Earth, Ocean and Atmospheric Sciences, Florida State University, Tallahassee, Florida, and LASG, Institute of Atmospheric Physics, Chinese Academy of Sciences, Beijing, China; Deng—School of Earth and Atmospheric Sciences, Georgia Institute of Technology, Atlanta, Georgia; van den Dool and Huang—NOAA/NWS/NCEP/Climate Prediction Center, College Park, Maryland; Ren—LASG, Institute of Atmospheric Physics, Chinese Academy of Sciences, Beijing, China; Saha and Wu—NOAA/NWS/NCEP/Environmental Modeling Center, College Park, Maryland
CORRESPONDING AUTHOR: Ming Cai, Dept. of Earth, Ocean and Atmospheric Science, Florida State University, 1017 Academic Way, Tallahassee, FL 32306
E-mail: mcai@fsu.edu

The abstract for this article can be found in this issue, following the table of contents.
DOI:10.1175/BAMS-D-14-00287.1

A supplement to this article is available online (10.1175/BAMS-D-14-00287.2)

In final form 6 October 2015

Motivated by the work cited above and referenced therein, we here propose a hybrid (dynamical plus statistical) paradigm for predicting the occurrence of individual continental-scale cold-air outbreaks (CAOs) in winter at the subseasonal range (0–30 days). As outlined in Fig. 1, the proposed hybrid paradigm is built on the following two premises: 1) the existence of robust diagnostic relationships between one or more indices that describe stratospheric circulation variability and indices of continental-scale CAOs at the surface and 2) the ability of operational models to predict the stratospheric indices used in the first premise 0–30 days in advance. Note that the temporal lead information in such a hybrid paradigm comes from dynamics/physics-based state-of-the-art operational models and the existence of precursor information in the statistical diagnostic component is not required. Therefore, the choice of such circulation indices is key for taking advantage of models' useful skill in the subseasonal range.

In the next section, we will discuss the rationales for the choices of the circulation indices in our deliberation on the feasibility of the proposed hybrid paradigm. The data, methods, and definitions section describes briefly the methods for deriving the circulation and CAO indices from standard outputs of operational models and historical data. The section on the association of CAOs with the strengthening of mass transport into the polar stratosphere is devoted to establishing the statistical relationship between the circulation and CAO indices. In the section on skill evaluations of forecasts for the ST60N, CNA, and CEA indices during the 2013/14 winter, we present evidence showing that the NCEP Climate Forecast System, version 2 (CFSv2; Saha et al. 2014) indeed possesses useful skill in predicting the circulation index at a range longer than 2 weeks in advance. The following section outlines a prototype procedure for real-time subseasonal forecasts of CAOs by combining the results presented earlier. The concluding remarks are provided in the final section of the paper. Detailed information on the skill evaluation and additional supporting evidences are provided in the online supplement to this paper (available online at http://dx.doi.org/10.1175/BAMS-D-14-00287.2).

RATIONALES FOR THE CHOICE OF CIRCULATION INDICES.

As reported in the literature (e.g., the references cited earlier), many stratospheric circulation indices, such as the northern annular mode (NAM), zonal mean zonal wind, polar vortex oscillation, eddy poleward heat flux (or the vertical component of the Eliassen–Palm flux), and streamfunction of the residual circulation

inferred from the downward control principle, may bear long-lead precursor information (0–60 days) for surface temperature anomalies. Such long-lead information has been utilized in statistical models for predicting monthly or seasonal mean surface temperature anomalies (e.g., Christiansen 2005; Siegmund 2005; Karpechko 2015). However, to the best of our knowledge, such statistical long-lead information has not been utilized for subseasonal forecasts of individual CAOs in a real-time (or operational) setting.

Because the temporal lead information for subseasonal forecasts of individual continental-scale CAOs in the hybrid paradigm comes from operational models' forecasts, we need to consider the following two requirements in selecting circulation indices: 1) they are predictable by operational models with a useful level of skill at a lead time longer than 2 weeks and 2) they are associated with dynamical processes that are physically responsible for individual CAOs. The second requirement above allows us to have a built-in causal relation in the statistical diagnostic component that links individual CAOs to circulation indices. Unlike monthly or seasonal mean temperature anomalies, the day-to-day variability of temperature anomalies is driven mainly by weather systems.

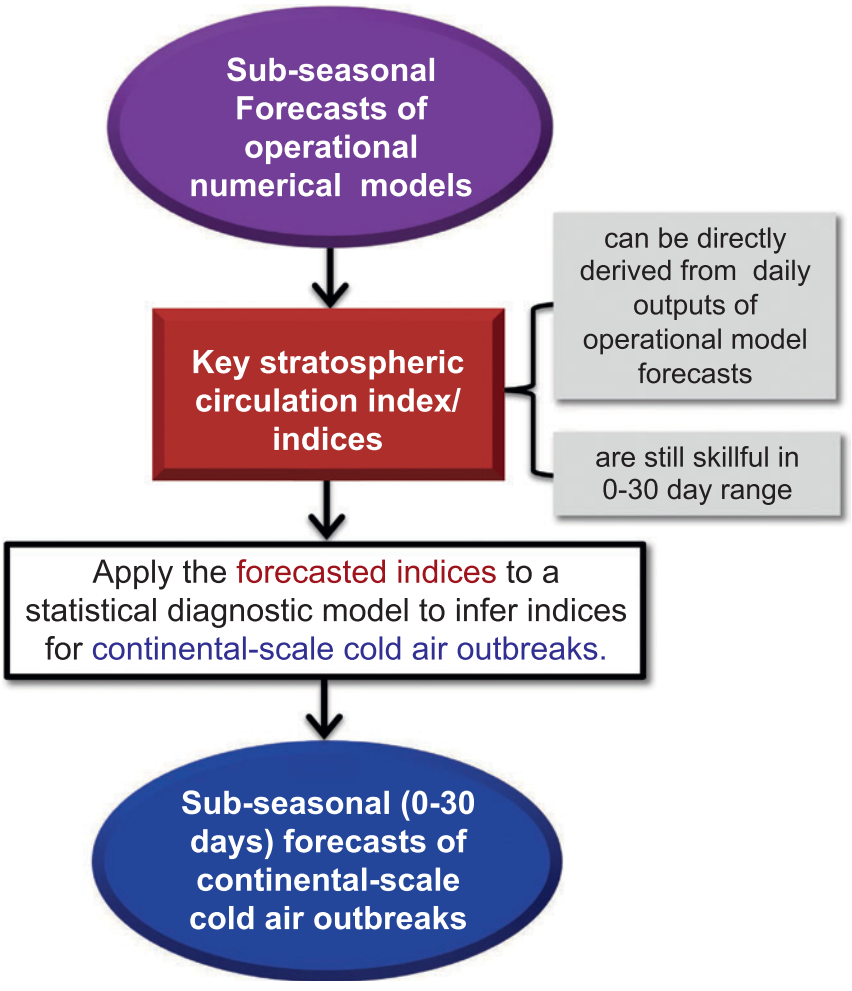

Fig. 1. Schematic showing the main components and the process flow of the proposed hybrid paradigm for subseasonal forecasts of continental-scale CAOs in the midlatitudes.

It has been shown in Yu et al. (2015a) that the timing of CAOs in midlatitudes is associated with the strengthening of equatorward cold airmass transport in the lower troposphere and the latter is nearly synchronized with the poleward warm-air transport in the upper atmosphere (including the stratosphere) into the polar region. Yu et al. (2015c) further showed that the anomalous intensification of surface weather systems that are responsible for CAOs is linked to the strengthening of the poleward warm-air transport in the upper atmosphere. The mechanism for the simultaneous poleward mass flux in upper-isentropic layers and equatorward mass flux below in the extratropics has been uniquely attributed to the dominance of westward-titled baroclinic waves (Johnson 1989). As a result of the hydrostatic and (quasi-) geostrophic balance, westward-tilted baroclinic waves always have a net poleward mass transport in upper levels and equatorward mass transport in lower levels. Intensification of westward-tilted waves results in a near-simultaneous increase in both the poleward mass transport into the polar region aloft and the equatorward discharge of the cold polar air mass in the lower troposphere, responsible for CAOs in the midlatitudes. Deep and large-amplitude baroclinic waves are capable of driving a strong meridional mass circulation that is connected to the stratosphere. Therefore, the stronger poleward mass transport in the extratropical stratosphere can be a robust indicator of the equatorward mass transport out of the

polar region in the lower troposphere [see sections 7 and 8 in Cai and Ren (2007) for the observational evidence]. This is the basis for the existence of the physical causal relationship between the mass circulation in the stratosphere and CAOs, which can be used as the statistical component of the hybrid paradigm for subseasonal forecasts of CAOs.

One of the advantages of using indices that measure the strength of the meridional mass circulation is that they can be independently and explicitly calculated from the instantaneous total flow without the need for decomposition into time mean and transient flows nor the separation into zonal mean and wave flows. Therefore, one can calculate mass circulation indices directly from the output fields of operational models once they are generated without waiting for forecast outputs at other lead times (or initial conditions) for averaging, which is essential for issuing forecasts in real time. Another advantage is that the variability of the annular modes (e.g., NAM and AO) can be physically explained and numerically accounted for from the isentropic meridional circulation variation (Yu et al. 2014, 2015b), but not from the residual circulation because the latter does not have convergence–divergence by construction, although the isentropic meridional mass circulation is nearly equivalent to the residual circulation in the time mean sense (Pauluis et al. 2011). The association of the meridional mass circulation with baroclinic waves depends on the amplitude of the waves, their westward-tilting structure, and their spatial scales, rather than the exact locations of a trough and ridge. Therefore, an operational forecast model would have skillful forecasts for the intensity of the meridional mass circulation as long as it can capture the amplitude and the spatial structure even though it cannot accurately predict the locations of the troughs and ridges of these waves (Zhang et al. 2013), a conjecture to be further substantiated in the section on the skill evaluations of forecasts for the ST60N, CNA, and CEA indices during the 2013/14 winter. The circulation indices that are constructed from EOF modes of anomaly fields, such as the NAM index, may not be predictable by operational models in the subseasonal range because the models' EOF modes are different from the observations in terms of both spatial patterns and explained variances (as well as their amplitude).

In this study, we consider indices that measure mass circulation intensity to illustrate the feasibility of subseasonal forecasts for CAOs in the midlatitudes in a real-time setting within the framework of the proposed hybrid paradigm. Since mass circulation intensity is directly related to temporal changes of mass fields (including the surface pressure tendency or the AO tendency), an anomalous intensification of mass circulation, which is referred to as a pulse, can be used as an indicator of a strong circulation event. We will use the total intensity of the stratospheric mass circulation predicted by operational models to detect the pulse and then use it in the statistical diagnostics model to forecast the occurrence probability of continental-scale CAOs in the midlatitudes.

DATA, METHODS, AND DEFINITIONS.

The information from the datasets used in this study, including their resolutions and main usages as well as their acronyms, are summarized in Tables 1 and 2. All data are daily data at 0000 UTC. Below are details of the methods used to derive meridional mass circulation indices with various isentropic surfaces as the bottom level and the cold temperature area indices from these daily data.

Indices of meridional mass circulation. The time and zonal mean mass circulation in isentropic coordinates is characterized by a single thermally direct circulation cell in each hemisphere that links the heat source in the tropics to the heat sink in high latitudes (e.g., Johnson 1989; Juckes et al. 1994; Held and Schneider 1999; Koh and Plumb 2004; Schneider 2005, 2006; Pauluis et al. 2008). Pauluis et al. (2011) further proposed a statistical transformed Eulerian mean (STEM) formulation for an easy diagnosis of the time mean meridional mass circulation. We here diagnose the zonal mean meridional isentropic mass

Table 1. List of the datasets and their acronyms used in this study.

Acronym	Full name	References
CFSR[a]	NCEP Climate Forecast System Reanalysis	Saha et al. (2010)
CFSv2	NCEP Climate Forecast System, version 2	Saha et al. (2014)
CFSRR[a]	CFSv2 Reforecasts	Saha et al. (2014)
NNR1[b]	NCEP–NCAR Reanalysis 1	Kalnay et al. (1996)

[a] Information online at http://nomads.ncdc.noaa.gov/data.php?name=access#cfsr.

[b] Information online at www.esrl.noaa.gov/psd/data/gridded/data.ncep.reanalysis.html.

Table 2. A brief summary of the datasets and their main uses.

Dataset	Date range	Horizontal resolution: Pressure	Horizontal resolution: Surface	Vertical resolution	Uses
CFSR	1 Dec 2013–28 Feb 2014	1° × 1°	T126 Gaussian grids	37 pressure levels from 1,000 to 1 hPa	Analysis of events during winter 2013/14
	1 Jan 1999–31 Dec 2009				CFSv2 forecast validation
CFSv2	1 Oct 2013–28 Feb 2014	1° × 1°	T126 Gaussian grids	37 pressure levels from 1,000 to 1 hPa	Skill analysis of CFSv2 forecasts
CFSRR	1 Jan 1999–31 Dec 2009	1° × 1°	T126 Gaussian grids	Surface air temperature field[a]	Systematic bias corrections for CFSv2 forecasts of surface air temperature
NNR1	1 Jan 1948–28 Feb 2014	2.5° × 2.5°	2.5° × 2.5°	17 pressure levels from 1,000 to 10 hPa	Climatological information of mass circulation and CAOs

[a] We only use the daily surface air temperature fields of the CFSRR dataset for bias corrections of CFSv2 forecasts of surface air temperature.

circulation on a daily basis. Following Pauluis et al. (2008), we interpolated the daily air temperature and wind fields onto 200 equally spaced sigma (σ) levels from 1 to 0. The air mass m_σ between two adjacent sigma surfaces per unit area is $m_\sigma = (\Delta\sigma/g)P_s$, where P_s is the surface pressure in pascals, g is the constant of gravity, and $\Delta\sigma = 1/200$. We then derived the zonally integrated meridional mass flux above a specific isentropic surface Θ_n at latitude ϕ on day t as

$$F_m(\phi,\Theta_n,t) = \int_0^{2\pi}\int_0^1 \left[m_\sigma(\lambda,\phi,t)\upsilon(\lambda,\phi,\sigma,t)\right]H\left[\theta(\lambda,\phi,\sigma,t)-\Theta_n\right]d\sigma d\lambda, \quad (1)$$

where l is longitude; $\upsilon(\lambda,\phi,\sigma,t)$ and $\theta(\lambda,\phi,\sigma,t)$ are the meridional wind and potential temperature fields, respectively; and $H(x)$ is the Heaviside function, such that $H(x) = 1$ for $x > 0$ and otherwise $H(x) = 0$.

In this study, we only consider the meridional mass transport into the region north of 60°N [i.e., only ϕ = 60°N in (1) is considered]. We have considered several values of Θ_n as the bottom level of a layer above the tropopause at 60°N: namely, Θ_n = 330, 350, 400, 450, 500, and 550 K. The results shown in the main text are obtained with Θ_n = 400 K: namely, ST60N = $F_m(\phi = 60°\text{N}, \Theta_n = 400\text{ K}, t)$, where ST stands for the stratospheric mass circulation. The results of other levels are shown and discussed in the online supplement to this paper.

Indices of cold areas over midlatitudes of North America and Eurasia. We now describe the method for indices measuring CAO activities over the midlatitudes (30°–60°N) of North America (120°–60°W) and Eurasia (0°–120°E). For a given dataset of daily surface air temperature (SAT) fields, we first calculate the climatological annual cycle ($\overline{\text{SAT}}$) by averaging the daily SAT field at each grid point across all available years of the daily SAT dataset for each calendar day from 1 December to 28 February. The corresponding daily anomalies are obtained by subtracting $\overline{\text{SAT}}$ from the total SAT. The resultant daily surface air temperature anomaly fields are denoted as SAT′. The local standard deviation (LSD) of SAT′ is derived from the long-time mean of the root-mean-square of SAT′ at each grid point for each day from 1 December to 28 February.

We calculate an index from SAT′ and LSD fields to measure the percentage of area occupied by cold (or negative) surface air temperature anomalies below $-\alpha \times$ LSD (denoted as C_α) according to

$$C\_\alpha = \frac{\int_{\phi_S}^{\phi_N}\int_{\lambda_W}^{\lambda_E} H\left(-\alpha\times\text{LSD}-\text{SAT}'\right)a\cos\phi d\lambda d\phi}{\int_{\phi_S}^{\phi_N}\int_{\lambda_W}^{\lambda_E} a\cos\phi d\lambda d\phi}, \quad (2)$$

where $\iint a\cos\phi d\lambda d\phi$ denotes an area integral over the domain specified in the integral, a is the mean radius of Earth, and $H(x)$ is the Heaviside function as in (1). We consider two cold temperature area indices for North America, denoted as CNA_α with α = 0.0 or 0.5, whose domains cover a latitude span from ϕ_S = 30°N to ϕ_N = 60°N and a longitude span from λ_W = 120°W to λ_E = 60°W. Similarly, we also consider two cold temperature area indices for Eurasia, denoted as CEA_α with α = 0.0 or 0.5, whose domains cover a latitude span from ϕ_S = 30°N to ϕ_N = 60°N and a longitude span from λ_W = 0° to λ_E = 120°E.

It follows that the CNA_0.0 (CNA_0.5) index is the percentage of area occupied by cold surface

air temperatures that are below the normal (below normal by at least 0.5LSD) over North America. The same thing can be said about CEA_0.0 and CEA_0.5, which are for Eurasia.

Definitions. Table 3 lists the percentile thresholds of ST60N, CNA_0.0, CNA_0.5, CEA_0.0, and CEA_0.5 derived from the National Centers for Environmental Prediction–National Center for Atmospheric Research (NCEP–NCAR) Reanalysis 1 (NNR1) during December–February (DJF) of 1948–2014. In this study, we refer to it as a strong event of mass transport across 60°N into the polar stratosphere or "a pulse of the stratosphere" (denoted as PULSE), when the ST60N index is above 6×10^9 kg s^{-1} (70th percentile) for at least n consecutive days (n = 2, 3, …, 8). Table 4 lists the total number of PULSEs, $M(n)$; their total number of days, $D(n)$; and the average peak intensity, PI(n), as a function of n during the period 1948–2014. It is seen that for n = 2, there are a total of 206 PULSEs in the 66 DJF or about 3 PULSEs per winter. This indicates that on average the hybrid paradigm would be able at most to forecast three rounds of CAOs based on the pulse information using this threshold value. Only one round of CAOs could be forecasted using the pulse information when the threshold for the duration is increased to 8 days. The fact that PI(n) increases as n increases implies that even if we use a constant intensity threshold for detecting PULSEs, we can use the duration days to indicate the intensity of a PULSE.

Individual CAOs are driven by mobile synoptic-scale weather systems. During a CAO event, cold-air temperature anomalies lie behind the troughs or in front of ridges, whereas warm temperature anomalies lie in front of troughs or behind ridges. Cold and warm temperature areas are relocated (eastward) as weather systems pass across a continent. Therefore, the condition that at least 50% area of a continent be occupied by cold temperature anomalies at any given day can be used to define a CAO event. Based on the discussion above, we refer to the condition that the daily value of a cold area index over a continent be above the Pth percentile (P = 50, 60, 70, 80, and 90) as a CAO event of intensity P over the continent. Using the notations for the four cold area indices defined in (2), we denote CNA_0.0_P and CNA_0.5_P for CAOs of intensity P over North America and CEA_0.0_P and CEA_0.5_P for CAOs of intensity P over Eurasia. One can easily infer the total number of days of CAOs of intensity P over a continent during the 66 DJF periods from the product of (1 − P%) and 5,940 (the total number of days in the 66 winter seasons).

ASSOCIATION OF CAOS WITH THE STRENGTHENING OF MASS TRANSPORT INTO THE POLAR STRATOSPHERE.

To illustrate the association of continental-scale CAOs with the strengthening of poleward mass transport into the polar stratosphere, we show in Fig. 2 the ST60N, CNA_0.0, CNA_0.5, CEA_0.0, and CEA_0.5 indices for the 2013/14 winter. It can be seen that there were three pronounced PULSEs (labeled as A, B, and D in Fig. 2a) with mass transport across 60°N into the polar stratosphere exceeding 6×10^9 kg s^{-1} for a week consecutively. The first two PULSEs were back-to-back week-long twin strong circulation events that started on 31 December 2013 with a peak intensity of 9.2×10^9 kg s^{-1} (above the 90th percentile). The PULSE D began on 31 January with a peak intensity of 11×10^9 kg s^{-1} (about 95th percentile) and lasted 8 days. Sandwiched between the twin and the third

Table 3. Percentile thresholds of the stratospheric mass circulation index and cold area percentage indices derived from NNR1 during the 66 DJFs from 1948 to 2014.

Percentile	ST60N (10^9 kg s^{-1})	CNA_0.0 (%)	CNA_0.5 (%)	CEA_0.0 (%)	CEA_0.5 (%)
Max	16.87	100	96.2	91.6	83.8
90th	8.28	77.4	60.5	70.7	51.2
80th	6.90	69.5	49.4	63.0	42.7
70th	5.96	62.8	41.0	56.8	37.3
60th	5.23	55.4	33.9	52.0	32.9
50th (median)	4.46	48.5	28.0	47.3	28.3
40th	3.96	41.7	22.4	42.9	24.4
30th	3.50	34.9	16.8	38.2	20.2
20th	2.90	28.0	11.4	32.9	15.8
10th	2.19	18.8	5.4	24.9	10.3
Min	−1.96	0	0	3.2	0

Table 4. Total number of PULSE events that last at least *n* consecutive days, their total number of days, and their average peak intensity (10^9 kg s^{-1}) recorded during the 66 DJFs of 1948–2014.

n	2	3	4	5	6	7	8
No. of events [*M*(*n*)]	206	178	154	135	117	101	76
Total No. of days during events [*D*(*n*)]	1,608	1,552	1,480	1,404	1,314	1,218	1,043
Avg peak intensity [PI(*n*)]	7.81	7.97	8.13	8.26	8.40	8.56	8.80

PULSEs was a minor PULSE (labeled as C), a 2-day event during 19 and 20 January 2014, whose peak just slightly exceeded 6×10^9 kg s^{-1} (70th percentile). Following the twin PULSEs A and B was a 14-day-long episode of CAOs in the midlatitudes of North America with 70%–80% of the area occupied by below-normal temperature anomalies or up to 60% of the area reporting below-normal temperature anomalies by at least half a standard deviation (both CNA_0.0 and CNA_0.5 exceeded the 90th percentile). A week-long massive CAO episode over North America with its cold area indices exceeding the 90th percentile followed PULSE D. Even the minor PULSE was followed by a 3-day-long weak CAO over North America. In the midlatitudes of Eurasia, however, there was only a 1-week-long episode of major CAO with the peak of CEA_0.0 or CEA_0.5 index reaching the 70th percentile level in the winter of 2013/14, which took place after the third pulse. It is important to point out that not all continental-scale CAOs are preceded by a stratospheric pulse, such as the major CAO that took place over the midlatitudes of North America during 9–21 December 2013. We have verified that during this period, there was little presence of large-amplitude planetary-scale waves in the stratosphere and, therefore, no strong circulation event in the stratosphere.

We next present statistical evidence supporting the idea that the relation between PULSEs and CAOs found in the 2013/14 winter holds for other years as well. To do this, we examine the occurrence probability of CAOs at different numbers of lead–lag days relative to the peak dates of PULSE events (Fig. 3) using the 66 yr of daily NNR1 data in DJF. For example, to construct the probability of the occurrence (PO) of CNA_0.0_P events, we count the total number of days of CNA_0.0_P events at t_0 days from the peak days of individual PULSEs, denoted as $N(t_0)$, with t_0 ranging from −10 to 25 days, where negative values of t_0 represent t_0 days before the peak days and positive values after. The PO of CNA_0.0_P at different lead–lag days relative to the peak dates of PULSEs is given by the ratio of $N(t_0)$ to the total number of PULSEs, $M(n)$, listed in the second row of Table 4, where n is the duration threshold for PULSE events. In the same fashion, we obtain the PO of CNA_0.5_P, CEA_0.0_P,

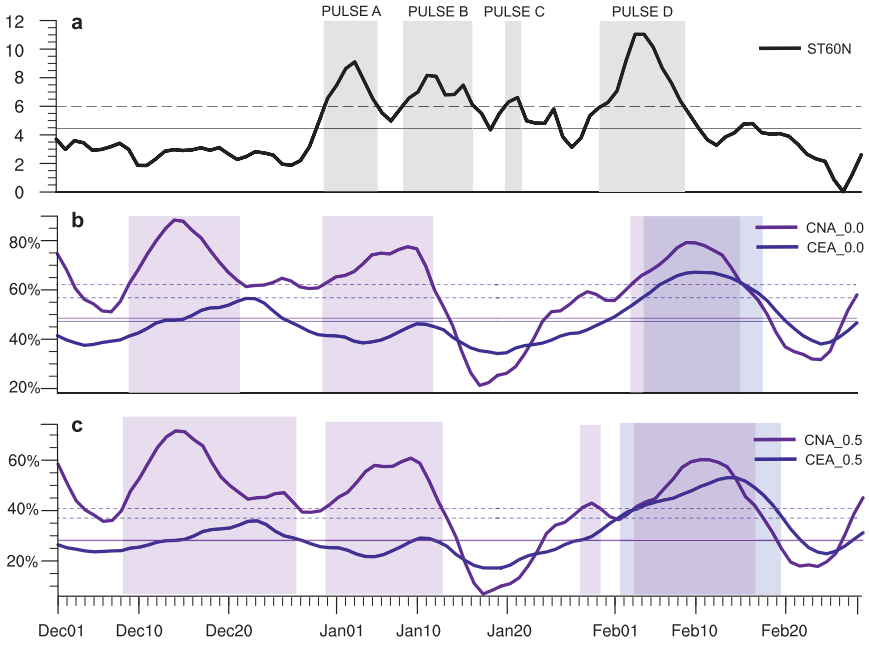

Fig. 2. Time series of various indices derived from the NOAA CFS Reanalysis (CFSR) for the period from 1 Dec 2013 to 28 Feb 2014. (a) The ST60N index (10^9 kg s^{-1}), (b) CNA_0.0 (purple) and CEA_0.0 (blue), and (c) the CNA_0.5 (purple) and CEA_0.5 (blue). The thin solid horizontal lines correspond to the median values of these indices (as shown in Table 2), while the dashed horizontal lines represent the 70th percentile thresholds of these indices. The shaded rectangular boxes in (a) mark the time spans of the four PULSE events—namely, the periods when ST60N exceeded the threshold of the 70th percentile—and those in (b) and (c) mark the time spans of CAO events defined by CNA 0.0_70, CEA 0.0_70, CNA 0.5_70, and CEA 0.5_70 (see text for details).

and CEA_0.5_P events at different numbers of lead–lag days relative to the peak dates of PULSEs.

To test the statistical significance of the PO of CAOs, we perform 5,000 Monte Carlo simulations using the same daily time series of CNA_0.0, CNA_0.5, CEA_0.0, and CEA_0.5. In each Monte Carlo simulation, we randomly select a set of $K(N)$ dates (N = 1–5,000) as the peak number of days of PULSEs in the 66-DJF period and evaluate the PO of CAOs at t_0 days from these randomly selected dates, with t_0 ranging from –10 to 25. We then rank the PO of CAOs at t_0 days from the peak days of the observed PULSEs against the 5,000 samples of the PO at t_0 days from the randomly selected dates. A statistical significance at the 5% level for the above-normal PO is determined when the observed PO of the CAOs at a given lead–lag time exceeds the 95th percentile of the 5,000 simulated POs at the same lead–lag time. Similarly, a statistical significance at the 5% level for the below-normal PO is determined when the observed value falls below the 5th percentile of the 5,000 simulated PO values. We have done two sets of 5,000 Monte Carlo simulations for each cold area index: one with two adjacent randomly selected dates at least 8 days apart and the other without such a condition. The statistical tests from the resultant Monte Carlo simulations are nearly identical.

We have obtained the POs of CNA_0.0_P, CNA_0.5_P, CEA_0.0_P, and CEA_0.5_P events with P = 50, 60, 70, 80, and 90 as a function of the number of lead–lag days relative to the peak dates of PULSE events with different duration thresholds, n. For the same value of P, the PO of CNA_0.0_P (CEA_0.0_P) is nearly identical to that of CNA_0.5_P (CEA_0.5_P). Therefore, it suffices just to show CNA_0.5_P and CEA_0.5_P, as displayed in Fig. 3 for P = 50 (for cold area indices above the 50th percentile) and P = 70 (for cold area indices above the 70th percentile). It is seen that the PO needed for CAOs to occur over Eurasia is significantly above the climatological probability during 1 week before the peak day of a PULSE. The peak PO of CEA_0.5_50 (CEA_0.5_70) events can be as high as 68% (44%) on day 3 (4) before the PULSE's peak day, which is a 36% (47%) gain from its climatology probability (equaling 1 − P%). The PO for CAOs to occur over North America becomes significantly above the climatology probability in the second week after the PULSE's peak day, with the peak probability of 63% (39%) on day 11 (16) for CNA_0.5_50 (CNA_0.5_70) events, a 26% (30%) gain from the climatological probability. The longer the duration (up to 8 days) of a PULSE is (which tends to be also a stronger PULSE), the higher the PO of the CAOs is. Comparison between the top and bottom panels of Fig. 3 indicates that the results are not sensitive to the threshold used for defining CAOs in terms of the timing information with respect to the peak days of PULSEs. However, the relative gain of the occurrence probability from the climatological probability is higher for more massive CAOs (detected by larger threshold P value). This implies that the skill

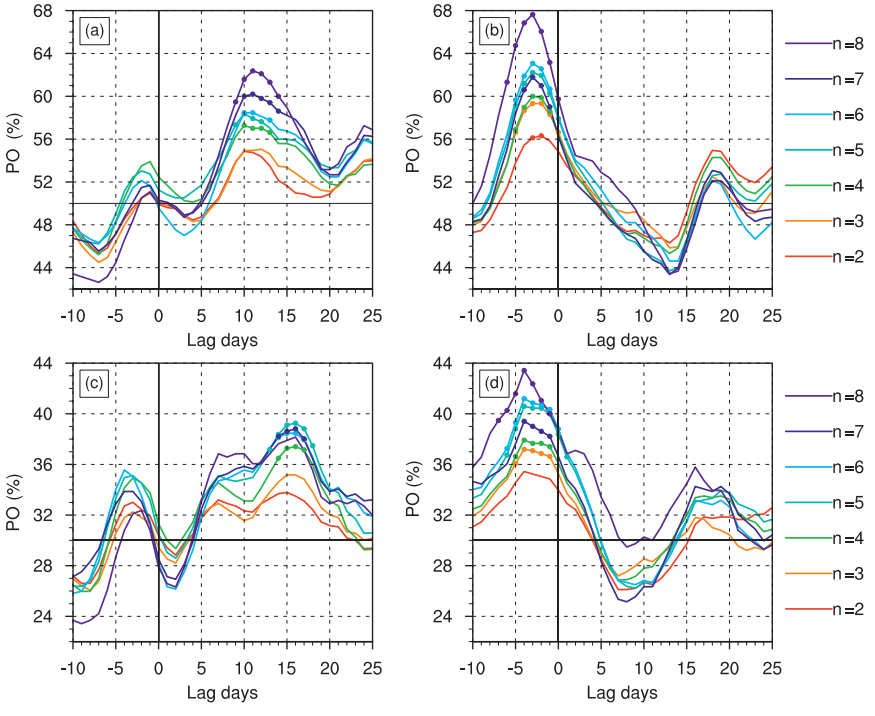

Fig. 3. Probability (solid color lines, %) of occurrence of (a) CNA 0.5_50, (b) CEA 0.5_50, (c) CNA 0.5_70, and (d) CEA 0.5_70 at different lead–lag times with respect to the peak dates of PULSEs with durations of *n* days or longer. Different colors correspond to different values of *n* (*n* = 2, 3, …, 8). The horizontal solid black line in each panel represents the climatological probability equaling the corresponding percentile threshold. The dots indicate statistical significance at the 5% level. Statistics are derived from the NNR1 dataset for the 66 DJFs of 1948–2014.

for relating CAOs to the peak days of PULSE is more robust for more massive CAOs.

We have constructed the PO of CAOs with respect to the peak days of PULSEs detected using different thresholds (the one for Fig. 3 is the 70th percentile threshold of the ST60N index). The timing information of the above-normal probability of CAOs is insensitive to the threshold value (as long as it is greater than the 60th percentile), as one may expect from the results of different duration time shown in Fig. 3 (recall that the duration time and intensity of a PULSE are positively correlated). We also have found that the larger the threshold intensity used to define a PULSE, the greater the above-normal probability for CAOs to occur, similar to the results of different duration times shown in Fig. 3. However, for a smaller threshold (say less than the 40th percentile), the diagnosed PO of CAOs approaches the climatological probability. Additional discussion of the threshold for detecting PULSE events is provided in the section offering a prototype hybrid paradigm for subseasonal forecasts of continental-scale CAOs.

SKILL EVALUATIONS OF FORECASTS FOR THE ST60N, CNA, AND CEA INDICES DURING THE 2013/14 WINTER. We now provide evidence suggesting that the CFSv2's operational forecasts during the 2013/14 winter did possess useful skill in predicting the ST60N index more than 2 weeks in advance, whereas their skill in directly predicting CAOs degrades significantly beyond 2 weeks. It is seen from Fig. 4a that similar to the observations, the ST60N derived from the CFSv2 forecasts at lead times of 1–50 days showed a below-normal mass transport into the polar stratosphere for most of December, and significantly above-normal mass transport in January and early February. The CFSv2 forecasts not only reproduced the general pattern of the temporal evolution, but also captured the occurrence of individual PULSE events. The useful skill of CFSv2 in forecasting PULSEs at the subseasonal range can also be seen from the time series of the ST60N derived from forecasts starting at a given initial condition, which is along the direction parallel to the dashed lines in Fig. 4a. Nevertheless, the timing of the forecasted PULSEs was delayed by up to a week or so in the CFSv2 forecasts at a lead time of 2 weeks and longer.

Figure 5a shows the correlation skill of the operational CFSv2 forecasts for the ST60N index during the winter of 2013/14 as a function of forecast lead time and lagged verification time. We consider a correlation of 0.3 to be the cutoff for "marginally useful" skill in the subseasonal range, a term that is borrowed from the experience in predictions of upper-level (i.e., 500-hPa height) charts in the 6–10-day range (e.g., Zhang et al. 2013; Hamill et al. 2004). In the opening section of the online supplement, we provide detailed information on how the correlation skill at a given forecast lead time is evaluated at different lagged verification times. By design, the correlation skill at zero lagged verification time is exactly equal to the convectional correlation skill. It is seen that CFSv2 does possess useful skill (above 0.4) in predicting the ST60N index even when the lead time is longer than 2 weeks, particularly in the range between 35 and 45 days. Moreover, the correlation skill in the range between 15 and 35 days is substantially improved when we verify the forecasts at an earlier time (positive lag, which attempts to account for the delay errors of the CFSv2 forecasts). This confirms that the overall correlation skill of the operational CFSv2 forecasts for the ST60N index during the winter of 2013/14 remained above the 0.5 level throughout the 45 days of lead time after the timing error, which is within the range of 1–10 days, had been taken into consideration. Therefore, the operational CFSv2 forecasts indeed possess useful prediction skill for the isentropic meridional mass circulation above 400 K (also see Fig. ES10b in the online supplement) at lead times of 30 days and longer. However, the CFSv2 forecasts for the meridional mass circulation below 400 K (Figs. ES9, ES11, and ES10a in the online supplement) are no longer reliable beyond 2 weeks.

From a forecaster's perspective, the "usefulness" or the actual skill that matters should be evaluated by following the lead-time series of the forecasted ST60N derived from the forecasts starting from the initial state when the forecast is made. In Fig. 4a, the real-time series of the forecasted ST60N is along the diagonal axis parallel to a dashed line, at which point the real time and forecast lead time are identical. It is seen that the twin PULSE events (PULSEs A and B) observed in the period of 1–15 January 2014 were detected by CFSv2 forecasts as early as 7 December 2013, which would provide forecasters useful information about the occurrence of PULSE events 20–40 days in advance. Similarly, the strongest PULSE event (PULSE D, 31 January–7 February 2014) observed in the 2013/14 winter was detected by CFSv2 forecasts as early as 26 December 2013, again within a lead time of 20–40 days. Moreover, these three major PULSE events showed up in most of the forecasts between the first detected data and their occurring dates except the obvious back-and-forth timing and duration errors of a few days. The combination of the back-and-forth timing errors and duration time errors make

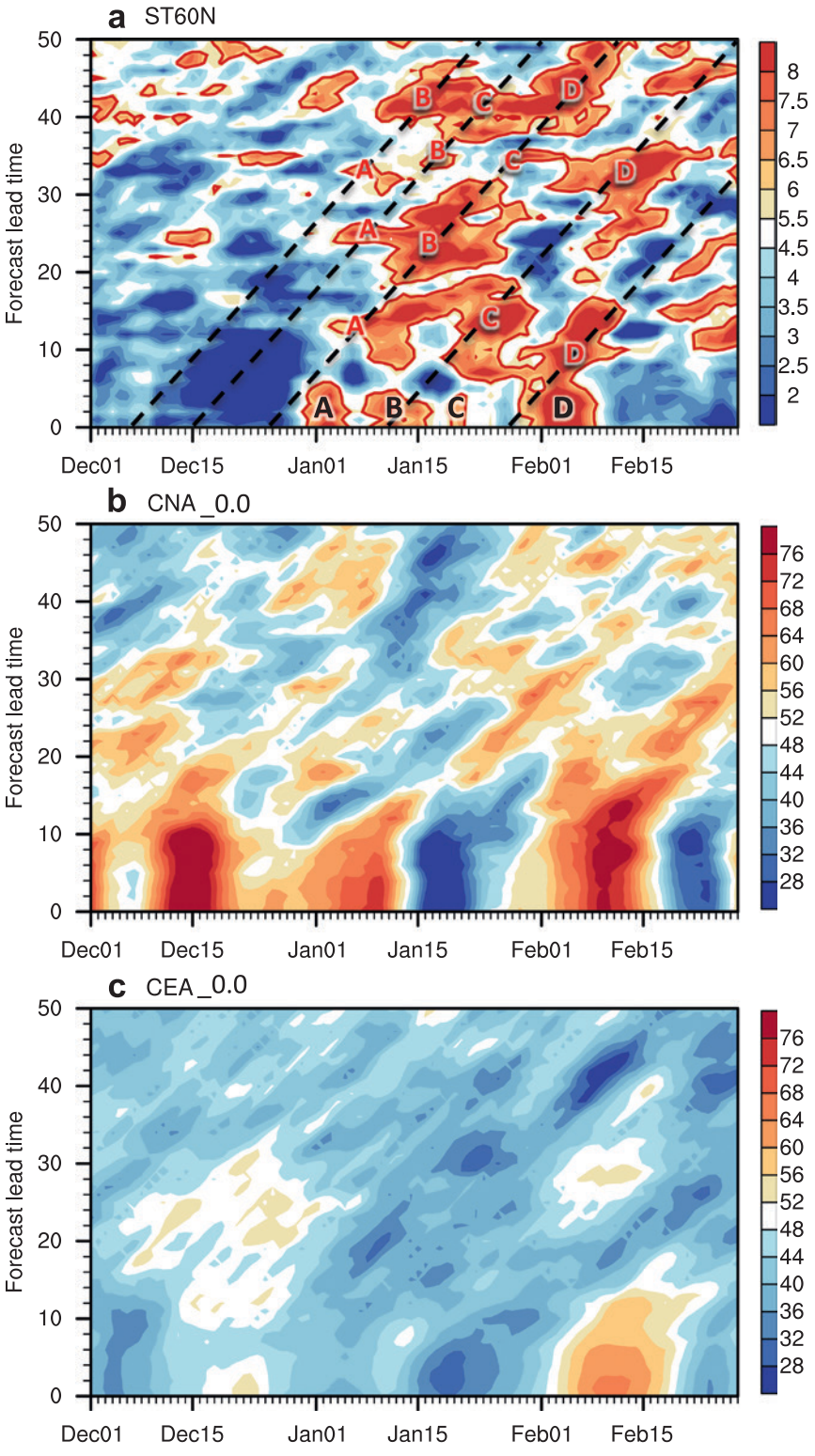

Fig. 4. Variations of various indices as a function of verification time (abscissa) during the 2013/14 winter and forecast lead time (ordinate): (a) ST60N (10^9 kg s^{-1}), (b) CNA_0.0 (%), and (c) CEA_0.0 (%). Day 0 in the lead time corresponds to the initial conditions of the CFSv2 forecasts. The white-shaded area corresponds to the climatological values derived from the NOAA CFSR for the period of 1999–2009. The dashed lines are along the diagonal axis at which the real time and forecast lead time are identical. The black-colored letters A–D mark the timing of the observed four PULSE events identified in Fig. 2, and those in red correspond to their counterparts detected from the five individual forecasts (i.e., the time series along the dashed lines).

the forecasted PULSEs appear "on" and "off" at the verification time, responsible for the relatively poor correlation skill at the verification time (i.e., the skill at lag 0 in Fig. 5a). It is important to point out that the PULSE C event, which was a 2-day PULSE event that just exceeded the threshold of PULSE events marginally, was not detected clearly until about 2 weeks before it happened. It appears that the difficulty in detecting the minor PULSE event from CFSv2 forecasts was mainly due to the large duration errors in forecasting the major PULSE B event that took place just a few days earlier. Therefore, CFSv2 can provide useful information for detecting large-amplitude PULSE events at a lead time of 20–40 days, except for timing and duration errors of a few days, but may not be able to do so for small-amplitude PULSE events. We will illustrate how to utilize the useful skill of the CFSv2 forecasts in detecting PULSEs 20–40 days in advance for real-time subseasonal forecasts of CAOs in the next section.

Turning our attention to the CFSv2 forecasts of CAOs, Fig. 4b shows that the CFSv2 forecasts were unable to capture the three massive CAOs over North

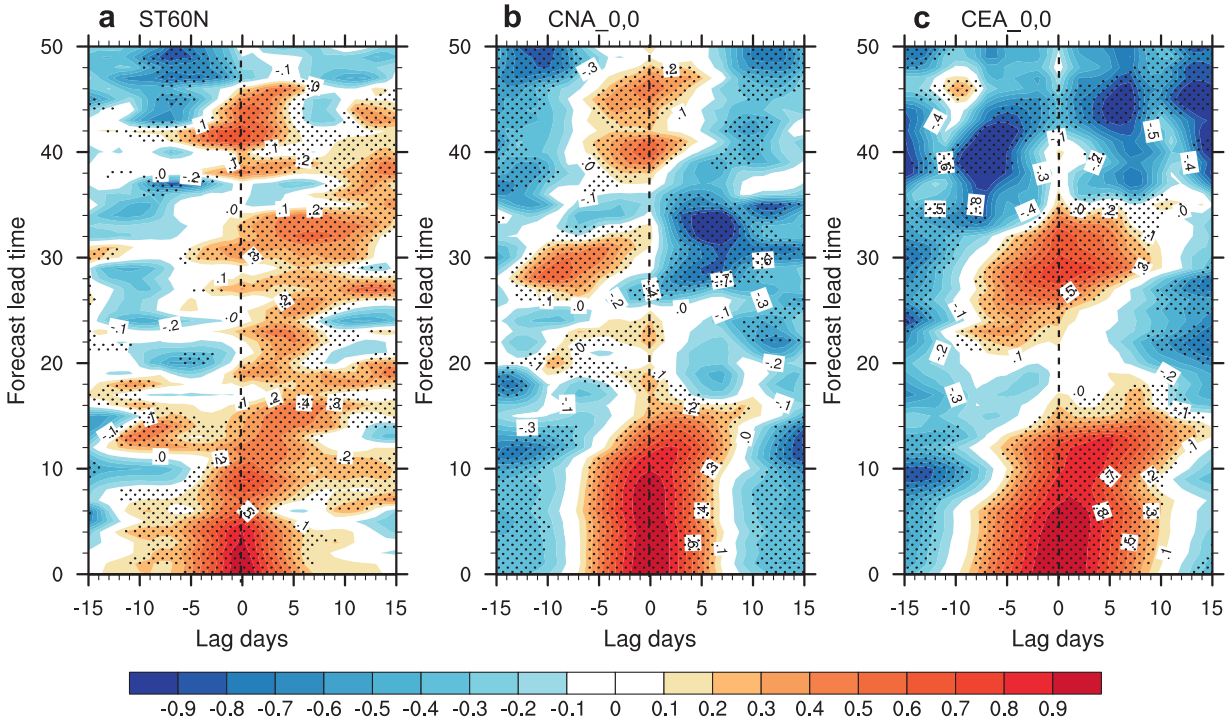

Fig. 5. The correlation scores of the operational CFSv2 forecasts for DJF 2013/14 as a function of the forecast lead time (ordinate, days) and lagged verification time (abscissa, days): (a) ST60N, (b) CNA_00, and (c) CEA_0.0. The dotted area indicates statistical significance at the 5% level.

America beyond 2 weeks. This was also the case for the sole prolonged massive CAO over Eurasia in the first half of February (Fig. 4c). Figures 5b and 5c vividly show the week 2 cutoff limit of the CFSv2 prediction skill for the CNA and CEA indices. Beyond 2 weeks, there is a lack of continuity in the correlation skill of the CFSv2 forecasts of these indices even after we have taken the timing error into consideration.

A PROTOTYPE HYBRID PARADIGM FOR SUBSEASONAL FORECASTS OF CONTINENTAL-SCALE CAOS. Figure 6 outlines an operationally implementable procedure for a hybrid (dynamical plus statistical) paradigm for real-time subseasonal forecasts of continental-scale CAOs. Before starting the operational subseasonal forecasts of CAOs, one needs to build the statistical component that links the pulse of the stratosphere to the occurrence probability of continental-scale CAOs of different levels of severity (i.e., in terms of area coverage over a continent and intensity), as shown in Fig. 3. One can construct such a statistical model for the occurrence probability of CAOs as a function of the intensity and duration of PULSEs. In operational forecasts, one can derive the ST60N index as a function of forecast lead time using the operational model's forecast outputs starting from the date when the forecasts for CAOs are to be made. PULSE events can be detected from the lead-time series of the forecasted ST60N index based on the forecaster's choice. The forecaster can issue forecasts for the temporal distribution of the high probability for CAOs of different severity to occur by plugging the information related to peak days, duration time, and intensity into the preconstructed statistical model.

In this hybrid forecast paradigm, one needs to consider the balance between "missing forecasts" and "false alarm" forecasts in choosing the threshold for detecting PULSEs for the model's forecast outputs. For a larger threshold, the PO of CAOs is higher and statistically more significantly above the climatology probability. However, one would have fewer CAO events to forecast because of the smaller number of PULSE events detected in the model's forecast outputs. This may yield more missing forecasts of CAO. On the other hand, a smaller threshold would lead to more PULSEs detected from the model's forecast. However, because 1) the model may not have useful skill in predicting small-amplitude PULSEs beyond 2 weeks and 2) the diagnostic information that links CAOs to PULSEs may not be statistically significant, a smaller threshold for PULSEs may lead to more false

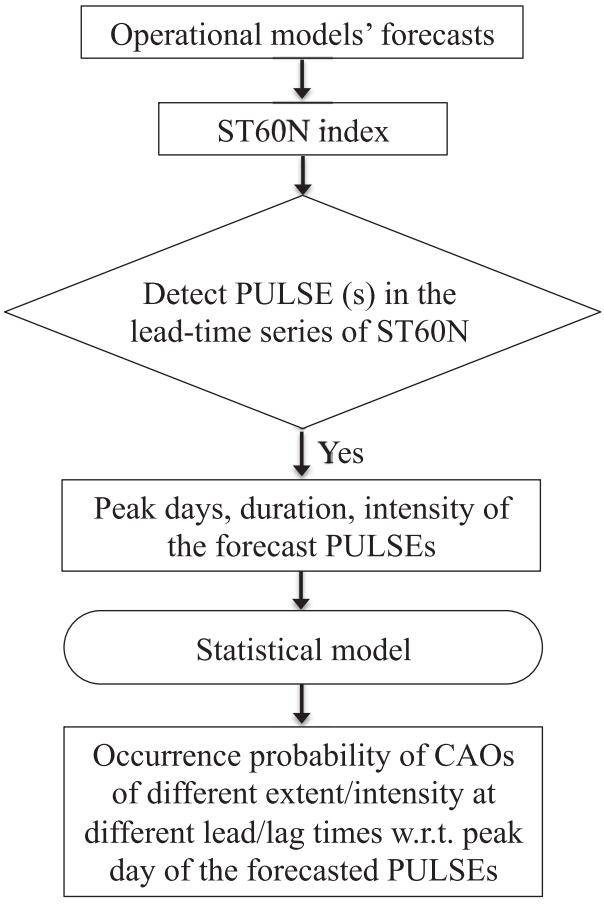

Fig. 6. Flowchart of the prototype hybrid paradigm for real-time subseasonal forecasts of continental-scale CAOs in the midlatitudes.

alarm detections of PULSE events from the model's forecast output and more false alarm forecasts of CAOS even when the model could capture small-amplitude PULSEs accurately.

We next wish to use the results presented in Figs. 4a and 3 to demonstrate how such a hybrid paradigm could be used for forecasting CAOs during the winter of 2013/14 at a lead time longer than 2 weeks. Because the twin PULSE (A and B) events first detected on 7 December 2013 remained above the threshold continuously in the later forecasts, one could forecast on 10 December 2013 about the high probability for CAOs to occur over the period a few days before the new year through the first 10 days of 2014, which would be a (at least) 25-day forecast. Since its detection on 7 December, the forecasted PULSE event appeared to show up at a later time in later forecasts until around 26 December when the timing delay of its occurrence in forecasts stopped. Therefore, one could issue a forecast on 26 December 2013 to predict that a new round of CAOs would occur during the period between the last week of January and the end of the second week of February. This would make it a 30-day forecast.

The feasibility of the prototype hybrid paradigm for predicting continental-scale CAOs in real time 1 month in advance has been put to a test at Florida State University by a team consisting of three graduate students and three undergraduate students led by the first author. They issued experimental subseasonal forecasts in real time, which are accessible freely by the general public and archived online (www.amccao.com). As recorded at the website, they were very successful in forecasting CAOs and winter storms at a lead time of 3–6 weeks in advance for the 2014/15 winter season. Specifically, they issued forecasts for a total of 15 PULSE events of strong mass transport into the polar stratosphere during the period from 14 October 2014 to 30 April 2015 at an average lead time of 1 month since 29 September 2014. All of their forecasts have been confirmed to capture the peak times of these 15 PULSEs within the time periods of their forecasts. There were only three major peaks of strong mass transport into the polar stratosphere that were not forecasted (29 November 2014, 10 December 2014, and 23 January 2015). None of the forecasts issued resulted in a false alarm. Most importantly, all of these 15 strong stratospheric circulation events (or PULSEs) were accompanied by major CAOs over at least one of the two major continents. This is particularly the case for North America where an abrupt increase in the area of below-normal temperatures was recorded within a few days after each of the 15 PULSEs. The inaugural subseasonal forecasts for CAOs during the winter of 2014/15 will be summarized in a separate paper.

CONCLUDING REMARKS. We have discovered that CAOs over the two major continents in the Northern Hemisphere on average tend to take place within a short time period from 1 week before to 1 to 2 weeks after anomalously strong mass transport into the polar stratosphere (i.e., the pulse of the stratosphere or PULSE). We also showed that an operational model, such as the CFSv2, is capable of predicting the PULSE, namely, the timing of strong mass transport into the polar stratosphere at a lead time of 20–40 days. This enables us to utilize the statistical relation between PULSE events and CAOs to predict the timing of having an abnormally high probability of the occurrence of continental-scale CAOs 1 month in advance.

In the online supplement to this paper, we have demonstrated that the key well-known polar stratospheric circulation indices, such as the

lower-stratospheric NAM index and polar stratospheric temperature anomalies, are dominated by low-frequency signals with long decorrelation time scales (about 3 weeks). From the mass circulation perspective, each PULSE event corresponds to a stronger poleward mass transport into the polar stratosphere, causing a rising in the polar stratospheric temperature and a decrease of the stratospheric NAM index. It often takes several consecutive PULSE events into the polar stratosphere to cause a substantial warming in the polar stratosphere and a substantial weakening of the polar stratospheric vortex. It follows that the low-frequency nature of the lower-stratospheric NAM index is a manifestation of the accumulative (or temporal integral) effect of multiple PULSE events. Furthermore, forecasts of PULSE events can be made all winter long, as we demonstrated in our experimental forecasts for the winter of 2014/15, since their success does not require the presence of stratospheric (major or minor) warming signals in the initial conditions, which is the case for the conventional strategy that relies solely on dynamical model forecasts (e.g., Sigmond et al. 2013; Tripathi et al. 2014).

We wish to add that only deep and large-amplitude baroclinic waves are capable of driving a stratospheric pulse that is connected to the troposphere. Therefore, the proposed hybrid prediction strategy may not be able to help predict continental CAOs associated with every anomalously strong tropospheric meridional circulation event nor cold events that are mainly created by underlying surface conditions (e.g., the "refrigerator" effect of snow cover).

It is noteworthy that the good skill found for the CFSv2 forecasts of PULSEs beyond the 2-week lead time for the 2013/14 winter was obtained without any systematic bias correction. The skill presented in Fig. 5a could be further improved after applying such bias corrections based on historical hindcasts made by the same model. Additionally, North American Multimodel Ensemble forecasts (Kirtman et al. 2014) may yield an even better level of skill for predicting PULSEs at a lead time longer than that obtained here, which is based on forecasts of a single model. Additionally, models with higher resolution may help to gain additional skill in predicting the stratospheric anomalies at a longer lead time (Marshall and Scaife 2010; Tripathi et al. 2014).

ACKNOWLEDGMENTS. The authors are grateful for the constructive and insightful comments from Dr. M. Alexander (the editor) and three anonymous reviewers that have led to a significant improvement in the presentation. MC is supported in part by research grants from the NOAA CPO/CPPA program (NA10OAR4310168), the National Science Foundation (AGS-1262173 and AGS-1354834), and the DOE Office of Science Regional and Global Climate Modeling (RGCM) program (DE-SC0004974). YYY is supported in part by research grants from the NOAA CPO/CPPA program (NA10OAR4310168) and the National Basic Research Program of China (2012CB417203). YD is supported by grants from the DOE Office of Science Regional and Global Climate Modeling (RGCM) program (DE-SC0005596) and the National Science Foundation (AGS-1147601, AGS-1354402, and AGS-1445956). RCR is supported by a research grant from the National Science Foundation of China (41430533, 41575041, and 91437105).

REFERENCES

Ambaum, M. H. P., and B. J. Hoskins, 2002: The NAO troposphere–stratosphere connection. *J. Climate*, **15**, 1969–1978, doi:10.1175/1520-0442(2002)015<1969:TNTSC>2.0.CO;2.

Baldwin, M. P., and T. J. Dunkerton, 1999: Propagation of the Arctic Oscillation from the stratosphere to the troposphere. *J. Geophys. Res.*, **104**, 30 937–30 946, doi:10.1029/1999JD900445.

——, and ——, 2001: Stratospheric harbingers of anomalous weather regimes. *Science*, **294**, 581–584, doi:10.1126/science.1063315.

——, and Coauthors, 2003: Stratospheric memory and skill of extended-range weather forecasts. *Science*, **301**, 636–640, doi:10.1126/science.1087143.

Cai, M., 2003: Potential vorticity intrusion index and climate variability of surface temperature. *Geophys. Res. Lett.*, **30**, 1119, doi:10.1029/2002GL015926.

——, and R.-C. Ren, 2007: Meridional and downward propagation of atmospheric circulation anomalies. Part I: Northern Hemisphere cold season variability. *J. Atmos. Sci.*, **64**, 1880–1901, doi:10.1175/JAS3922.1.

Charlton, A. J., and L. M. Polvani, 2007: A new look at stratospheric sudden warmings. Part I: Climatology and modeling benchmarks. *J. Climate*, **20**, 449–469, doi:10.1175/JCLI3996.1.

Christiansen, B., 2005: Downward propagation and statistical forecast of the near-surface weather. *J. Geophys. Res.*, **110**, D14104, doi:10.1029/2004JD005431.

Douville, H., 2009: Stratospheric polar vortex influence on Northern Hemisphere winter climate variability. *Geophys. Res. Lett.*, **36**, L18703, doi:10.1029/2009GL039334.

Gerber, E. P., C. Orbe, and L. M. Polvani, 2009: Stratospheric influence on the tropospheric circulation

revealed by idealized ensemble forecasts. *Geophys. Res. Lett.*, **36**, L18703, doi:10.1029/2009GL040913.

Hamill, T. M., J. S. Whitaker, and X. Wei, 2004: Ensemble reforecasting: Improving medium-range forecast skill using retrospective forecasts. *Mon. Wea. Rev.*, **132**, 1434–1447, doi:10.1175/1520-0493(2004)132<1434:ERIMFS>2.0.CO;2.

Hardiman, S. C., and Coauthors, 2011: Improved predictability of the troposphere using stratospheric final warmings. *J. Geophys. Res.*, **116**, D18113, doi:10.1029/2011JD015914.

Hartley, D. E., J. T. Villarin, R. X. Black, and C. A. Davis, 1998: A new perspective on the dynamical link between the stratosphere and troposphere. *Nature*, **391**, 471–474, doi:10.1038/35112.

Haynes, P. H., 2005: Stratospheric dynamics. *Annu. Rev. Fluid Mech.*, **37**, 263–293, doi:10.1146/annurev.fluid.37.061903.175710.

——, M. E. McIntyre, T. G. Shepherd, C. J. Marks, and K. P. Shine, 1991: On the "downward control" of extratropical diabatic circulations by eddy-induced mean zonal forces. *J. Atmos. Sci.*, **48**, 651–678, doi:10.1175/1520-0469(1991)048<0651:OTCOED>2.0.CO;2.

Held, I. M., and T. Schneider, 1999: The surface branch of the zonally averaged mass transport circulation in the troposphere. *J. Atmos. Sci.*, **56**, 1688–1697, doi:10.1175/1520-0469(1999)056<1688:TSBOTZ>2.0.CO;2.

Holton, J. R., P. H. Haynes, M. E. McIntyre, A. R. Douglass, R. B. Rood, and L. Pfister, 1995: Stratosphere-troposphere exchange. *Rev. Geophys.*, **33**, 403–439, doi:10.1029/95RG02097.

Johnson, D. R., 1989: The forcing and maintenance of global monsoonal circulations: An isentropic analysis. *Advances in Geophysics*, Vol. 31, Academic Press, 43–316, doi:10.1016/S0065-2687(08)60053-9.

Juckes, M. N., I. N. James, and M. Blacburn, 1994: The influence of Antarctica on the momentum budget of the southern extratropics. *Quart. J. Roy. Meteor. Soc.*, **120**, 1017–1044, doi:10.1002/qj.49712051811.

Kalnay, E., and Coauthors, 1996: The NCEP/NCAR 40-Year Reanalysis Project. *Bull. Amer. Meteor. Soc.*, **77**, 437–471, doi:10.1175/1520-0477(1996)077<0437:TNYRP>2.0.CO;2.

Karpechko, A. Y., 2015: Improvements in statistical forecasts of monthly and two-monthly surface air temperatures using a stratospheric predictor. *Quart. J. Roy. Meteor. Soc.*, **141**, 2444–2456, doi:10.1002/qj.2535.

Kidston, J., A. A. Scaife, S. C. Hardiman, D. M. Mitchell, N. Butchart, M. P. Baldwin, and L. J. Gray, 2015: Stratospheric influence on tropospheric jet streams, storm tracks and surface weather. *Nat. Geosci.*, **8**, 433–440, doi:10.1038/ngeo2424.

Kirtman, B. P., and Coauthors, 2014: The North American Multimodel Ensemble: Phase-1 seasonal-to-interannual prediction; phase-2 toward developing intraseasonal prediction. *Bull. Amer. Meteor. Soc.*, **95**, 585–601, doi:10.1175/BAMS-D-12-00050.1.

Kodera, K., and Y. Kuroda, 1990: Downward propagation of upper stratospheric mean zonal wind perturbation to the troposphere. *Geophys. Res. Lett.*, **17**, 1263–1266, doi:10.1029/GL017i009p01263.

Koh, T. Y., and R. A. Plumb, 2004: Isentropic zonal average formalism and the near-surface circulation. *Quart. J. Roy. Meteor. Soc.*, **130**, 1631–1653, doi:10.1256/qj.02.219.

Kolstad, E. W., T. Breiteig, and A. A. Scaife, 2010: The association between stratospheric weak polar vortex events and cold air outbreaks in the Northern Hemisphere. *Quart. J. Roy. Meteor. Soc.*, **136**, 886–893, doi:10.1002/qj.620.

Kuroda, Y., 2008: Role of the stratosphere on the predictability of medium-range weather forecast: A case study of winter 2003–2004. *Geophys. Res. Lett.*, **35**, L19701, doi:10.1029/2008GL034902.

——, 2010: High initial-time sensitivity of medium-range forecasting observed for a stratospheric sudden warming. *Geophys. Res. Lett.*, **37**, L16804, doi:10.1029/2010GL044119.

Li, J.-P., and R.-Q. Ding, 2011: Temporal–spatial distribution of atmospheric predictability limit by local dynamical analogs. *Mon. Wea. Rev.*, **139**, 3265–3283, doi:10.1175/MWR-D-10-05020.1.

Limpasuvan, V., and D. L. Hartmann, 2000: Wave-maintained annular modes of climate variability. *J. Climate*, **13**, 4414–4429, doi:10.1175/1520-0442(2000)013<4414:WMAMOC>2.0.CO;2.

Marshall, A. G., and A. A. Scaife, 2010: Improved predictability of stratospheric sudden warming events in an atmospheric general circulation model with enhanced stratospheric resolution. *J. Geophys. Res.*, **115**, D16114, doi:10.1029/2009JD012643.

——, ——, and S. Ineson, 2009: Enhanced seasonal prediction of European winter warming following volcanic eruptions. *J. Climate*, **22**, 6168–6180, doi:10.1175/2009JCLI3145.1.

Mitchell, D. M., L. J. Gray, J. Anstey, M. P. Baldwin, and A. J. Charlton-Perez, 2013: The influence of stratospheric vortex displacements and splits on surface climate. *J. Climate*, **26**, 2668–2682, doi:10.1175/JCLI-D-12-00030.1.

Pauluis, O., A. Czaja, and R. Korty, 2008: The global atmospheric circulation on moist isentropes. *Science*, **321**, 1075–1078, doi:10.1126/science.1159649.

——, T. Shaw, and F. Laliberté, 2011: A statistical generalization of the transformed Eulerian-mean circulation for an arbitrary vertical coordinate system. *J. Atmos. Sci.*, **68**, 1766–1783, doi:10.1175/2011JAS3711.1.

Perlwitz, J., and N. Harnik, 2003: Observational evidence of a stratospheric influence on the troposphere by planetary wave reflection. *J. Climate*, **16**, 3011–3026, doi:10.1175/1520-0442(2003)016<3011:OEOASI>2.0.CO;2.

Polvani, L. M., and D. W. Waugh, 2004: Upward wave activity flux as a precursor to extreme stratospheric events and subsequent anomalous surface weather regimes. *J. Climate*, **17**, 3548–3554, doi:10.1175/1520-0442(2004)017<3548:UWAFAA>2.0.CO;2.

Ren, R.-C., and M. Cai, 2007: Meridional and vertical out-of-phase relationships of temperature anomalies associated with the northern annular mode variability. *Geophys. Res. Lett.*, **34**, L07704, doi:10.1029/2006GL028729.

Saha, S., and Coauthors, 2010: The NCEP Climate Forecast System Reanalysis. *Bull. Amer. Meteor. Soc.*, **91**, 1015–1057, doi:10.1175/2010BAMS3001.1.

——, and Coauthors, 2014: The NCEP Climate Forecast System version 2. *J. Climate*, **27**, 2185–2208, doi:10.1175/JCLI-D-12-00823.1.

Schneider, T., 2005: Zonal momentum balance, potential vorticity dynamics, and mass fluxes on near-surface isentropes. *J. Atmos. Sci.*, **62**, 1884–1900, doi:10.1175/JAS3341.1.

——, 2006: The general circulation of the atmosphere. *Annu. Rev. Earth Planet. Sci.*, **34**, 655–688, doi:10.1146/annurev.earth.34.031405.125144.

Shepherd, T. G., 2002: Issues in stratosphere-troposphere coupling. *J. Meteor. Soc. Japan*, **80**, 769–792, doi:10.2151/jmsj.80.769.

Siegmund, P., 2005: Stratospheric polar cap mean height and temperature as extended-range weather predictors. *Mon. Wea. Rev.*, **133**, 2436–2448, doi:10.1175/MWR2985.1.

Sigmond, M., J. F. Scinocca, V. V. Kharin, and T. G. Shepherd, 2013: Enhanced seasonal forecast skill following stratospheric sudden warmings. *Nat. Geosci.*, **6**, 98–102, doi:10.1038/ngeo1698.

Smith, D. M., A. A. Scaife, and B. P. Kirtman, 2012: What is the current state of scientific knowledge with regard to seasonal and decadal forecasting? *Environ. Res. Lett.*, **7**, 015602, doi:10.1088/1748-9326/7/1/015602.

Song, Y., and W. A. Robinson, 2004: Dynamical mechanisms for stratospheric influences on the troposphere. *J. Atmos. Sci.*, **61**, 1711–1725, doi:10.1175/1520-0469(2004)061<1711:DMFSIO>2.0.CO;2.

Stan, C., and D. M. Straus, 2009: Stratospheric predictability and sudden stratospheric warming events. *J. Geophys. Res.,* **114**, D12103, doi:10.1029/2008JD011277.

Thompson, D. W. J., and J. M. Wallace, 2001: Regional climate impacts of the Northern Hemisphere annular mode. *Science*, **293**, 85–89, doi:10.1126/science.1058958.

——, M. P. Baldwin, and J. M. Wallace, 2002: Stratospheric connection to Northern Hemisphere wintertime weather: Implications for prediction. *J. Climate*, **15**, 1421–1428, doi:10.1175/1520-0442(2002)015<1421:SCTNHW>2.0.CO;2.

Tripathi, O. P., and Coauthors, 2014: The predictability of the extratropical stratosphere on monthly timescales and its impact on the skill of tropospheric forecasts. *Quart. J. Roy. Meteor. Soc.*, **141**, 987–1003, doi:10.1002/qj.2432.

Yoden, S., K. Ishioka, D. Durran, T. Enomoto, Y.-Y. Hayashi, T. Miyoshi, and M. Yamada, 2014: Theoretical aspects of variability and predictability in weather and climate systems. *Bull. Amer. Meteor. Soc.*, **95**, 1101–1104, doi:10.1175/BAMS-D-14-00009.1.

Yu, Y.-Y., R.-C. Ren, J.-G. Hu, and G.-X. Wu, 2014: A mass budget analysis on the interannual variability of the polar surface pressure in winter season. *J. Atmos. Sci.*, **71**, 3539–3553, doi:10.1175/JAS-D-13-0365.1.

——, M. Cai, R.-C. Ren, and H. van den Dool, 2015a: Relationship of warm air mass transport into upper polar atmosphere and cold air outbreaks in winter. *J. Atmos. Sci.*, **72**, 349–368, doi:10.1175/JAS-D-14-0111.1.

——, R.-C. Ren, and M. Cai, 2015b: Comparison of the mass circulation and AO indices as indicators of cold air outbreaks in northern winter. *Geophys. Res. Lett.*, **42**, 2442–2448, doi:10.1002/2015GL063676.

——, ——, and ——, 2015c: Dynamical linkage between cold air outbreaks and intensity variations of the meridional mass circulation. *J. Atmos. Sci.*, **72**, 3214–3232, doi:10.1175/JAS-D-14-0390.1.

Zhang, Q., C.-S. Shin, H. van den Dool, and M. Cai, 2013: CFSv2 prediction skill of stratospheric temperature anomalies. *Climate Dyn.*, **41**, 2231–2249, doi:10.1007/s00382-013-1907-5.

AMS BOOKS

RESEARCH | APPLICATIONS | HISTORY

AMS MEMBERS GET FREE

CLIMATE

The Thinking Person's Guide to Climate Change

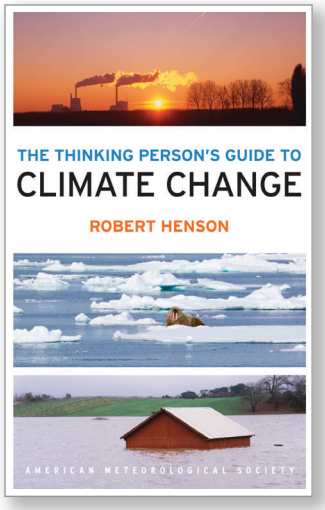

ROBERT HENSON

This fully updated and expanded revision of The *Rough Guide to Climate Change* combines years of data with recent research. It is the most comprehensive overview of climate science, acknowledging controversies but standing strong in its stance that the climate is changing—and something needs to be done.

© 2014, PAPERBACK, 520 PAGES,
ISBN: 978-1-935704-73-7
LIST $30 MEMBER $20

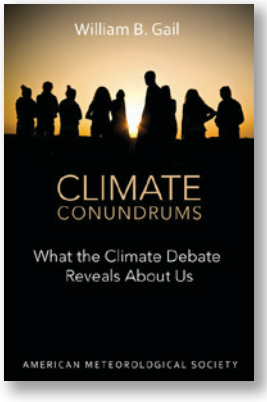

Climate Conundrums:
What the Climate Debate Reveals about Us

WILLIAM B. GAIL

This is a journey through how we think, individually and collectively, about humanity's relationship with nature, and more. Can we make nature better? Could science and religion reconcile? Gail's insights on such issues help us better understand who we are and find a way forward.

© 2014, PAPERBACK, 240 PAGES,
ISBN: 978-1-935704-74-4 LIST $30 MEMBER $20

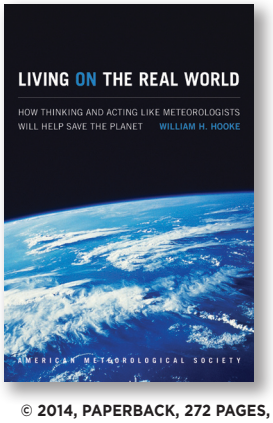

Living on the Real World:
How Thinking and Acting Like Meteorologists Will Help Save the Planet

WILLIAM H. HOOKE

Meteorologists focus on small bits of information while using frequent collaboration to make decisions. With climate change a reality, William H. Hooke suggests we look to the way meteorologists operate as a model for how we can solve the 21st century's most urgent environmental problems.

© 2014, PAPERBACK, 272 PAGES, ISBN 978-1-935704-56-0 LIST $30 MEMBER $22

GUIDES

An Observer's Guide to Clouds and Weather:
A Northeastern Primer on Prediction

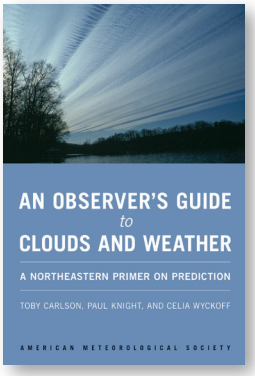

TOBY CARLSON, PAUL KNIGHT, AND CELIA WYCKOFF

With help from Penn State experts, start at the beginning and go deep. This primer, intended for both serious enthusiasts and new meteorology students, will leave you with both refined observation skills and an understanding of the complex science behind the weather: the ingredients for making reliable predictions of your own. It connects fundamental meteorological concepts with the processes that shape weather patterns, and will make an expert of any dedicated reader.

© 2014, PAPERBACK, 210 PAGES,
ISBN: 978-1-935704-58-4 LIST $30 MEMBER $20

Eloquent Science:
A Practical Guide to Becoming a Better Writer, Speaker, and Atmospheric Scientist

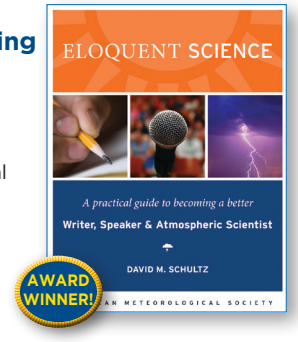

DAVID M. SCHULTZ

The ultimate communications manual for undergraduate and graduate students as well as researchers in the atmospheric sciences and their intersecting disciplines.

© 2009, PAPERBACK, 440 PAGES,
ISBN 978-1-878220-91-2

LIST $45 MEMBER $30

TEXTBOOK

Midlatitude Synoptic Meteorology:
Dynamics, Analysis, and Forecasting

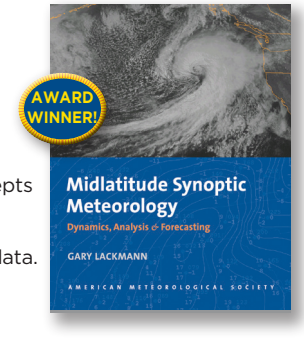

GARY LACKMANN

This textbook links theoretical concepts to modern technology, facilitating meaningful application of concepts, theories, and techniques using real data.

©2011, PAPERBACK, 360 PAGES,
ISBN 978-1-878220-10-3
LIST $100 MEMBER $75 STUDENT MEMB. $65

Midlatitude Synoptic Meteorology Teaching CD
More than 1,000 PowerPoint Slides.
© 2013, CD, ISBN 978-1-878220-27-1 LIST $100 MEMBER $75

To order: bookstore.ametsoc.org, 617-226-3998, or use the order form in this magazine

SHIPPING + DISCOUNTS AT BOOKSTORE.AMETSOC.ORG

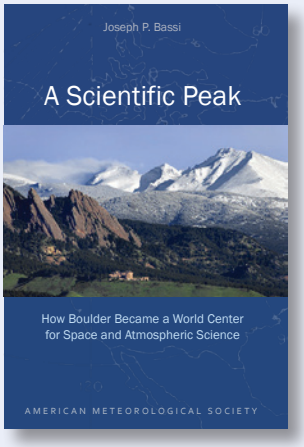

A Scientific Peak:

How Boulder Became a World Center for Space and Atmospheric Science

JOSEPH P. BASSI

How did big science come to Boulder, Colorado? Joe Bassi introduces us to the characters, including Harvard sun–Earth researcher Walter Orr Roberts, and the unexpected brew of politics, passion, and sheer luck that during the Cold War era transformed this "Scientific Siberia" to home of NCAR and NOAA.

© 2015, PAPERBACK, 264 PAGES, ISBN: 978-1-935704-85-0

LIST PRICE: $35.00 MEMBER PRICE: $25.00

METEOROLOGICAL MONOGRAPH SERIES

AMS Meteorological Monographs Vols. 1–55 (1947–2010) are available via Springer at springer.com/ams, with select volumes available in print via AMS at bookstore.ametsoc.org. Starting in 2016 with Vol. 56, new monographs will be open access, available via the AMS Journals Online site.

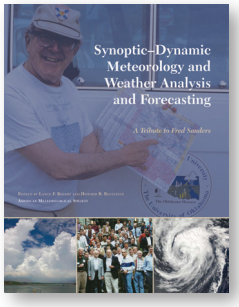

Synoptic–Dynamic Meteorology and Weather Analysis and Forecasting:

A Tribute to Fred Sanders

EDITED BY LANCE F. BOSART AND HOWARD B. BLUESTEIN

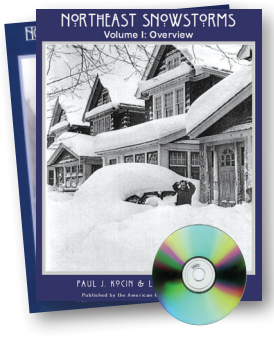

Northeast Snowstorms

(Volume I: Overview, Volume II: The Cases)

PAUL J. KOCIN AND LOUIS W. UCCELLINI

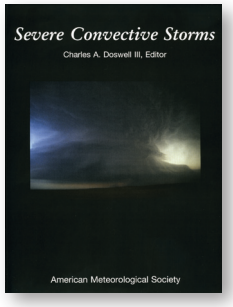

Severe Convective Storms

EDITED BY CHARLES A. DOSWELL III

Booksellers, groups, or for examination copies:
The University of Chicago Press:
1-800-621-2736 (US & Canada)
773-702-7000 (all others)
custserv@press.uchicago.edu

HISTORY

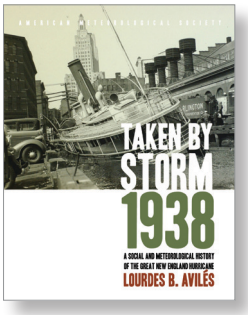

Taken by Storm, 1938:

A Social and Meteorological History of the Great New England Hurricane

LOURDES B. AVILÉS

The science behind the 1938 Hurricane, which hit New England unannounced, is presented here for the first time along with new data that sheds light on the motivations of the Weather Bureau forecasters. This compelling history successfully weaves science, historical accounts, and social analyses to create a comprehensive picture of the most powerful and devastating hurricane to hit New England to date.

© 2013, HARDCOVER, 288 PAGES, ISBN: 978-1-878220-37-0

LIST $40 MEMBER $30

Father Benito Viñes:

The 19th-Century Life and Contributions of a Cuban Hurricane Observer and Scientist

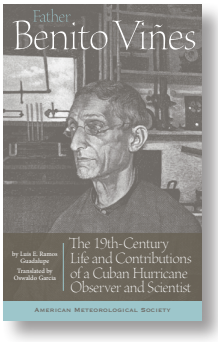

LUIS E. RAMOS GUADALUPE

TRANSLATED BY OSWALDO GARCIA

Before Doppler radar and weather broadcasts, Spanish Jesuit Benito Viñes (1837–1893) spent decades observing the skies at Belen Observatory in colonial Cuba. Nicknamed "the Hurricane Priest," Viñes taught the public about the weather and developed the first network of weather observation stations in the Caribbean, groundwork for the hurricane warning systems we use today.

© 2014, PAPERBACK, 172 PAGES
ISBN: 978-1-935704-62-1 LIST $20 MEMBER $16

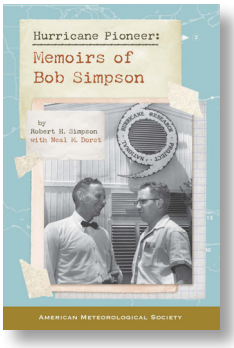

Hurricane Pioneer:

Memoirs of Bob Simpson

ROBERT H. SIMPSON AND NEAL DORST

In 1951, Bob Simpson rode a plane into a hurricane—just one of the many pioneering exploits you'll find in these memoirs. Bob and his wife Joanne are meteorological icons: Bob was the first director of the National Hurricane Research Project and a director of the National Hurricane Center. He helped to create the Saffir–Simpson Hurricane Scale; the public knows well his Categories 1–5. Proceeds from this book help support the AMS's K. Vic Ooyama Scholarship Fund.

© 2015, PAPERBACK, 156 PAGES
ISBN: 978-1-935704-75-1 LIST $25 MEMBER $20

AMS
American Meteorological Society

GIFTS EVEN A FAIR WEATHER FAN WOULD LOVE

Visit the AMS online bookstore for gift ideas for fans of all weather.
www.ametsoc.org/amsbookstore

Back to School Special - 10% discount*
Use code: FALL16
Offer valid 9/2–10/31

*eligible products

Orders may also be made by check/money order or by submitting Visa, MC, or AMEX information.
Call 617-226-3998, Fax 617-742-8718, or mail your payment to AMS, 45 Beacon Street, Boston, MA 02108.